A Reliability-Optimised Maximum Power Point Tracking Algorithm and Neural Network Lifetime Prediction for Photovoltaic Power Converters

Niall Andrew Smith supervised by Mahmoud Shahbazi

***Abstract*—The reliability of power converters in photovoltaic systems is critical to the overall system reliability. This paper proposes a novel active thermal controlled algorithm that aims to reduce the rate of junction temperature increase, therefore increasing the reliability of the device. The algorithm works alongside a normal perturb & observe maximum power point tracking algorithm. In conjunction with a neural network, the algorithm is applied to long term real mission profile data. The proposed algorithm resulted in a 3.3 % reduction in lifetime consumption with a 1.0 % reduction in total energy generated. There is a demonstrated trade-off between lifetime consumption reduction and energy generated reduction. The results are also split by day type. Under very variable conditions, the algorithm resulted in a 4.4 % reduction in lifetime consumption with a 1.4 % reduction in total energy generated. Lifetime consumption was predicted with greater than 96.5 % accuracy. Energy generated was predicted with greater than 99.5 % accuracy. The neural network, when applied to 365 days of data was 28 times faster than using standard electrothermal modelling.**

***Index Terms*—Solar PV, Lifetime Improvement, Regression Neural Networks, Active Thermal Control, MPPT.**

I. Introduction

IN 2021, the Intergovernmental Panel on Climate Change published the AR6 report which stated that humans have had an "unequivocal" influence on warming the planet [1], and predicts global temperature rise to exceed 1.5 °C above pre-industrial levels before 2050 unless action is taken [2]. Already, it is "virtually certain" that extreme weather has become more frequent and intense as a direct result of human influence with high confidence that this will worsen with increased temperatures. Limiting the rise to 1.5 °C requires deep emissions reduction in all sectors.

Looking specifically at the United Kingdom, the UK government committed to a net-zero greenhouse gas emission target by 2050 [3]. The UK's Climate Change Committee estimates that by 2050, 50-75 % of overall energy production in the UK will be generated by variable renewables, including solar photovoltaic (PV), for which the generation capacity of 14 GW in 2022 is expected to increase by 145-615 GW [4], [5]. Consequently, if solar PV is to play a role in the decarbonisation of power generation as needed, it is paramount that PV technology continues to develop.

Maximising energy production from the PV panel is needed to offset the manufacturing price. However, this is often at the cost of decreasing the reliability of the system [6]. PV arrays are typically subject to harsh environments involving several stressors, such as high temperatures, vibrations, and high humidity. In a survey conducted with industry experts, thermal stressors were thought of as the most critical for PV power converters, both through losses and power cycling [7], [8]. Over a 5 year operational period of a large PV plant in Tucson, AZ, USA, 37 % of unscheduled maintenance events were related to inverters, accounting for 59 % of unscheduled maintenance costs [9]. 40 % of survey respondents considered power semiconductors to be the most important area of research for improving reliability, further highlighting the devices' critical nature in the reliability of power electronics. The majority of respondents wished to see more research into active methods for improving system reliability.

Active Thermal Control (ATC) is utilised as an active method for reducing the damage accumulated from thermal cycling, with several techniques being suggested within power electronics research [10]. An important part of ATC methods in power electronics is an accurate estimation of the junction temperature. Andresen *et al.* [11] gives a review of current temperature measurement and estimation techniques and several implementation possibilities of ATC are described. The ATC methods discussed apply to power semiconductors in all applications, rather than specifically grid-connected PV. The authors in [12] also provide an overview of junction temperature measurement and estimation techniques.

Some literature uses temperature-sensitive electrical properties for temperature estimation [13]. For example, Xu *et al.* [14] proposed a method whereby the IGBT current is measured during a short circuit pulse, with the short circuit current being directly linked to junction temperature. The results showed a good ability to predict and calculate temperature, however this method requires additional hardware for measurement. Meanwhile, Motto and Donlon [15] included temperature sensing integrated into a power module by utilising the forward voltage drop on several diodes directly fabricated onto the semiconductor die. As the forward voltage drop of a diode is related linearly to diode temperature, this can be used to estimate the junction temperature. This comes at the cost of added module complexity.

Analytical electrothermal models are also used widely within literature to predict temperature, without the need for measurement hardware [6], [16], [17]. In [16], system-level reliability and lifetime prediction of grid-connected PV

systems were discussed, for which an electrothermal model is employed. A rainflow counting algorithm is used to find temperature cycles from the electrothermal model, with cycles to failure calculated using the Coffin-Manson law. This procedure is common and well-documented within literature.

One application for an ATC technique in a PV systems is proposed by Andresen *et al.* [6], with a "lifetime-optimised" Perturb & Observe (P&O) Maximum Power Point Tracking (MPPT) algorithm which works to reduce thermal stress during highly variable conditions and limits the power semiconductor junction temperature. The proposed algorithm was modelled and tested against an unchanged algorithm, with electrothermal model junction temperatures verified with laboratory work. Results showed lifetime was improved by 13% while sacrificing 3.7% of potential energy generation when the proposed algorithm was employed. Different parameters were tested, which demonstrated a direct trade-off between energy generation and lifetime reduction. However, the mission profile is not field data and was created based upon the analysis of real irradiance data, rather than directly using real irradiance data. Additionally, simulations were only run on a mission profile lasting 10 minutes.

A study of lifetime of semiconductor devices in a PV system under real long-term mission profiles lasting a year is reported in [18]. For this, several look-up tables are utilised. A key part of this paper is the inclusion of device degradation feedback, where increases in the thermal resistance are accounted for with feedback based on the current estimated device degradation level. The paper concludes that device degradation feedback is important for accurate long-term lifetime estimation, with a 20-30% reduction in actual lifetime versus a model without feedback. The results also showed the importance of operating region on reliability.

Felgemacher *et al.* [17] evaluate the impact of thermal stress cycling in PV inverters with varying cooling strategies. Similar to [18], look-up tables were used to speed up computation times. Mission profiles from various locations were simulated. It was shown that cooling strategy can play a large role in ensuring the reliability of inverters, especially in high irradiance areas such as the Earth's Sunbelt. This paper analyses heatsink temperature. However, this may miss important failure mechanisms from the junction temperature cycles, as the thermal capacity of the semiconductor is much lower than that of the heatsink, causing much more pronounced temperature cycles. It is not clear how large of an effect the cooling strategy has on junction temperature.

In [19], the authors use a statistical approach for IGBT failure analysis is used after electrothermal modelling of a PV system. This is based on Monte Carlo simulations, as physical tolerances and operational stresses will vary by component. Probability distribution functions for key electrical and lifetime model parameters are used to find the sensitivity to accumulated damage. Statistical lifetime analysis is then performed, giving a lifetime with a specified confidence level. The paper discusses changing the electrothermal parameters, such as thermal resistance as the device ages, as is carried out in [18].

Peyghami *et al.* [20] introduces a novel power converter lifetime performance indicator, employing an Artificial Neural Network (ANN) to replace the detailed electrothermal model. The paper addresses the lack of easily available long-term reliability performance indicators, allowing for better reliability-orientated design and maintenance planning. The converter reliability is represented as lines of constant lifetime, plotted with active/reactive power. Monte Carlo reliability analysis is performed to estimate the B_{10} lifetime of the converter, similar to [19]. The ANN is designed through trial and error, with the final design of 4 hidden layers. The use of ANNs decreased the required time of lifetime calculation by a factor of 5. Converter electrothermal modelling is used to train the ANN, and lifetime predictions are found by applying the neural network to a converter mission profile. The ANN could accurately predict the lifetime of a converter, with less than 5% error compared to traditional stress-strength analysis.

Current research in the area of power converter reliability, and more specifically grid-connected PV power converters, implement look-up tables to shorten computation times. The accuracy of results is dependent on the size of the look-up table, and these papers are often using mission profiles that is not real irradiance data. Additionally, current literature uses simulations of short duration that do not accurately show the results over a long period of time, and do not reflect the true results if the systems were implemented in the field. This paper aims to apply a neural network to a novel active thermal control P&O MPPT algorithm trained using electrothermal models. Using an neural network would allow for long-term real irradiance data sets to be used without extensive and time-consuming simulations, without significantly compromising accuracy, granting a better understanding of real-world trade-offs between energy generated and lifetime improvement when using the ATC algorithm.

In Section II, the PV electrothermal model is described, and the theory governing power converter lifetime is given. Section III describes the method whereby neural networks are implemented in a way to circumvent extensive electrothermal simulations. In Section IV, an active thermal control algorithm is proposed. Section V discusses the implementation and details of the PV electrothermal model and neural network training. Finally, Section VI presents the results of the study.

II. Electrothermal Lifetime Modelling

This section details the theory behind simulating an electrothermal PV model and converting temperature readings into device lifetime consumption values. As shown in [7]–[9], power converters are often the most unreliable components in grid-connected PV systems.

Section II-A shows the grid-connected PV electrical system model used in this paper. Equations for IGBT and anti-parallel diode power losses are given. The Foster thermal model used for junction temperature estimation is shown.

The junction temperature is analysed to estimate the lifetime consumption of the IGBT device using a Coffin-Manson law and the Miner's rule, with the procedure given in Section II-B.

A. Electrothermal Modelling

Connecting an inherently DC PV system to the grid can be achieved in many ways [6], [18], [21]. The differences in implementation result from the level of control and complexity desired. However, most structures use an MPPT-controlled DC/DC stage, with a DC/AC stage connected to the grid. This paper considers a simple structure that has been documented well within literature.

A 10 kW, 2-stage, single-phase, transformer-less grid-connected PV system is used in this paper. The topology can be seen in Figure 1. The first stage is a boost converter controlled by an MPPT algorithm for maximum power extraction. The second stage is a full-bridge grid-connected inverter, which maintains the DC link voltage and exports AC power to the grid, at the correct voltage and phase. An LCL filter ensures the output grid current reaches a total harmonic distortion of less than 5 % [22].

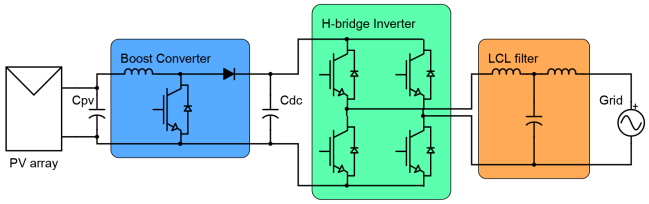

Fig. 1. Grid-connected PV array connection topology under study, using a two-stage structure.

Power loss in the IGBT is calculated using Equation 1, where the total power loss is the sum of the conduction (P_{cond}) and switching (P_{sw}) losses. Where conduction losses are calculated with collector-emitter voltage V_{ce}, collector current I_c, and duty cycle D. Switching losses are calculated with switching frequency f_{sw}, energy loss during turn on E_{on}, and turn off E_{off} [23].

$$P_{total} = \underbrace{V_{ce} \cdot I_c \cdot D}_{P_{cond}} + \underbrace{f_{sw} \cdot (E_{on} + E_{off})}_{P_{sw}} \quad (1)$$

Power loss in the diode is calculated using Equation 2. Similarly to IGBTs, power loss is split into conduction and switching losses. Conduction losses are based on the forward bias V_F, forward current I_F and resistance R_D. Switching losses are calculated with reverse recovery charge Q_{RR} and reverse bias V_R [24], [25].

$$P_{loss} = \underbrace{V_F \cdot I_{F,avg} + R_D \cdot I_{F,rms}^2}_{P_{cond}} + \underbrace{\frac{f_{sw} \cdot Q_{RR} \cdot V_R}{3}}_{P_{sw}} \quad (2)$$

Semiconductor junction temperature is the temperature of the semiconductor material within the transistor. In this paper, junction temperature is analysed as it is a direct contributor to device degradation and failure. As the semiconductor material is contained within the outer device case, measuring the temperature is non-trivial with Section I giving an overview of current temperature measurement techniques. For the analysis in this paper, a Foster thermal model is employed to find junction temperatures, with the structure shown in Figure 2 [26]. Foster thermal models have been applied multiple times within literature, and while may not provide a direct link to reality like Cauer thermal models, they are much easier to implement [6], [16], [17].

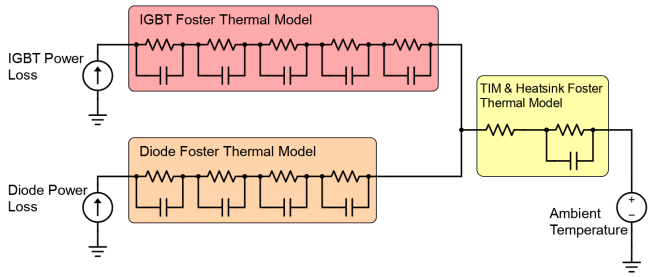

Fig. 2. Foster thermal model used for predicting junction temperatures. IGBT and diode foster thermal parameters are statistical fits for measured thermal data, with no physical significance [26].

IGBT and diode Foster thermal model values are provided by the IGBT manufacturer. Thermal Interface Material (TIM) & heatsink values are taken from parts. TIM thermal capacitance is neglected.

B. Lifetime Consumption Estimation

This section details the procedure used for estimating the device lifetime consumption based on junction temperature data. This method has been well documented in literature, especially in conjunction with an electrothermal model [6], [10], [18], [19].

Temperature cycling comes in two forms: short term and long term. Short term temperature cycling is primarily due to the line frequency, as seen in Figure 3. This is a result of the sinusoidal currents generated from the inverter. Short term cycling typically occurs on a scale less than 1 s. Long term temperature cycling, on the scale of a few seconds and greater generally results from irradiance or ambient temperature changes.

The raw junction temperature samples from the electrothermal model are first analysed by finding the peaks and valleys, as seen in Figure 4. This removes a lot of unnecessary data, reducing the required computation for the next stage. The isolated peaks and valleys are then analysed using a rainflow counting algorithm, which will extract the temperature cycle amplitude, average cycle temperature and cycle count. The output of the rainflow counting algorithm can be used in estimating the number of cycles to failure, described by Equation 3. This equation, described in [27], encompasses many IGBT failure mechanisms.

$$N_f = K \cdot \Delta T_j^{\beta_1} \cdot exp(\frac{\beta_2}{T_j + 273}) \cdot t_{on}^{\beta_3} \cdot I^{\beta_4} \cdot V^{\beta_5} \cdot D^{\beta_6} \quad (3)$$

Where K is a constant term, t_{on} is the heating time, I is the current per bond wire, V is the voltage class of IGBT, and D is the diameter of bond wire. The temperature swing ΔT_j, absolute temperature T_j, and t_{on} can be seen in

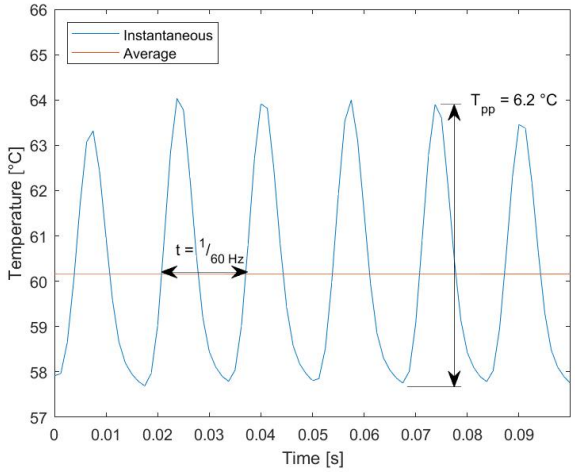

Fig. 3. An example of short term junction temperature cycling. Cycles occur at 60 Hz due to inverter loading. Peak to peak junction temperature cycle amplitude changes depending on inverter power output. Due to the number of cycles over a day, these cycles form the bulk of the lifetime consumption.

Figure 4. The model parameters β_1 to β_6 used in this paper are given in [27].

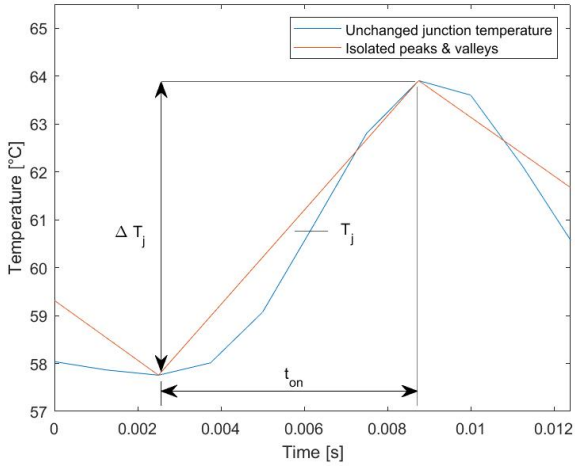

Fig. 4. Short term line-frequency temperature cycle with isolated peaks and valleys shown. Some of the key variables in Equation 3 are labelled.

The accumulated Lifetime Consumption (LC) of the power converter can then be calculated using the Miner's rule [28]:

$$LC = \sum_i \frac{n_i}{N_{fi}} \tag{4}$$

Where n_i is the number of thermal cycles, and N_{fi} is the expected cycles to failure, calculated in Equation 3. The output, lifetime consumption (LC), is the sum of damages from each cycle. When LC surpasses 1, the device is predicted to have reached the end of its life. This model does not take into account statistical tolerances on components or the increase in thermal resistance R_{th} with device degradation.

Using the procedure outlined in this section, Section III describes the implementation of a regression neural network for the prediction of lifetime consumption values, removing the requirement for the electrothermal modelling described in this section.

III. Neural Network Regression of Lifetime Consumption

Neural networks are mimic mathematical abstractions of the human brain. The structure of the network can be adjusted to optimise for different computational tasks such as numerical prediction or classification. Regression neural networks, used for making numerical predictions, are common data tools for non-linear functions. Neural networks have been applied to similar lifetime predictions [20]. Other methods of lifetime estimation include look-up tables, however accuracy is limited by the size of look-up table [6]. Neural networks are proposed as a method of lifetime consumption prediction, reducing the requirement for extensive long term electrothermal modelling while achieving higher accuracy than look-up tables.

Regression networks are implemented in MATLAB using fitrnet. Fitrnet trains a feed-forward, fully connected neural network designed for regression. Two separate neural networks were used, estimating energy generation (EG) and lifetime consumption (LC). A single multiple output neural network was found to be inaccurate, as network training performance metrics could not train a network accurately for multiple outputs as energy generation is comparatively easier to predict than lifetime consumption, which biased the performance metric. The structure of the neural networks used can be seen in Figures 6 and 7.

The irradiance data is sampled at a rate of once per minute. A moving window is used that predicts the energy generation and lifetime consumption within the next minute. This is shown in Figure 8. This allows the network to be applied to days of any length, days of interrupted data, as well as reducing the total amount of inputs, consequently reducing computation.

Energy generation in the next minute is predicted using the current irradiance value and cell temperature. Lifetime consumption in the next minute is predicted using the current irradiance, ambient temperature, as well as irradiance values for the minutes on either side. The reasoning for lifetime consumption inputs is focused on the junction temperature. The heat capacitance of the device and heatsink means the junction temperature is not only a function of the current irradiance but also the previous and next irradiance values. A demonstration of the heat capacitance can be seen in Figure 12, where the temperature is not an abrupt step as with irradiance.

The hidden layer structure was found through trial and error. Other network parameters such as regularisation, standardisation and activation function were found through hyperoptimisation.

The workflow of data, showing the process of training and applying neural networks is shown in Figure 5. The training data represents a selected sample of the long term mission profile data used to train the networks. The training of the networks requires input and target values. The target values are the output of the electrothermal model. The input values

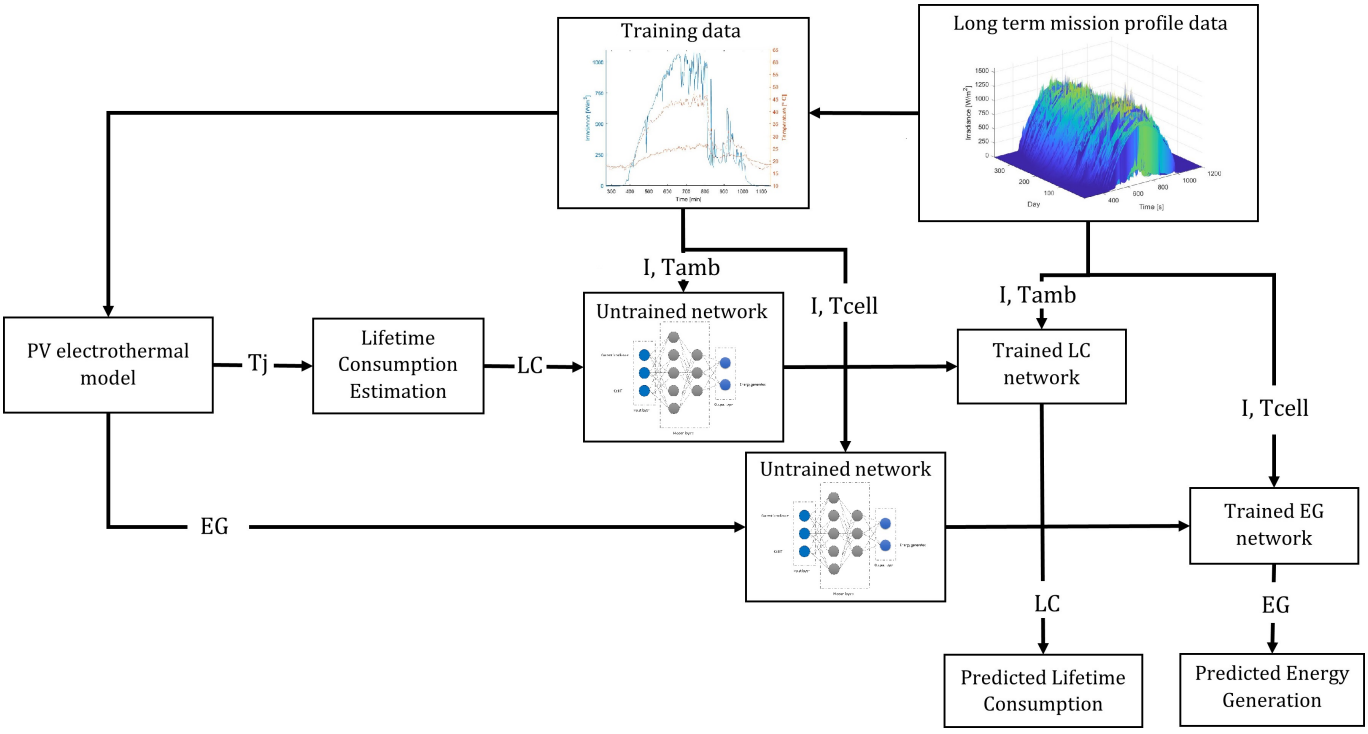

Fig. 5. Workflow showing electrothermal model and lifetime consumption estimation being used to train networks, with the trained networks later being applied to long term data.

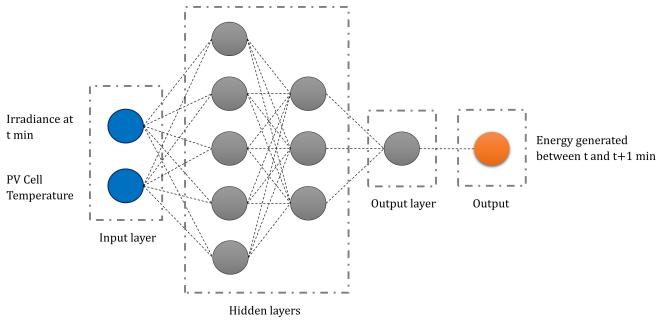

Fig. 6. Visualisation of neural network structure for predicting energy generation. Hidden layer structure of [5, 3] not final. Weights, biases and activation functions are not shown. The activation function for the hidden layers is given in Section V. Output layer activation function is linear.

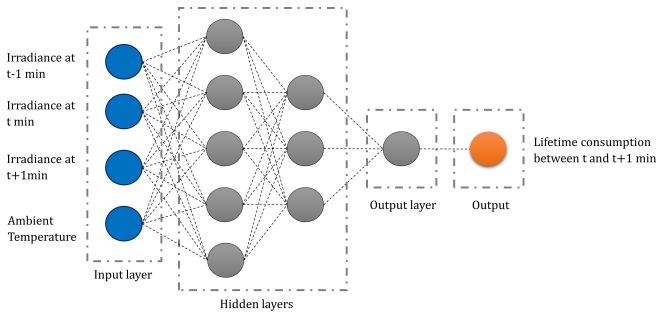

Fig. 7. Visualisation of neural network structure for predicting lifetime consumption. Hidden layer structure of [5, 3] not final. Weights, biases and activation functions are not shown. The activation function for the hidden layers is given in Section V. Output layer activation function is linear.

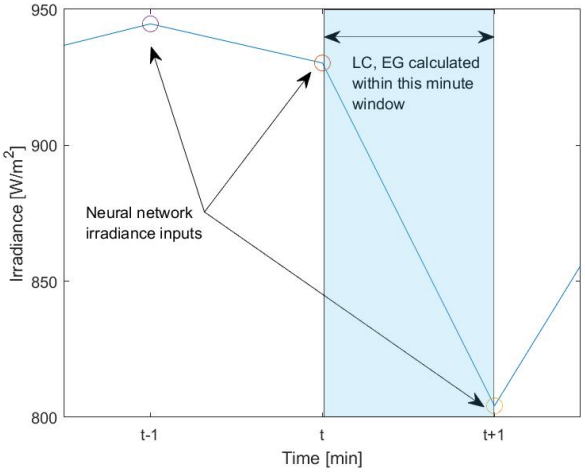

Fig. 8. Irradiance values applied to the neural networks, showing the window from t min to t+1 min in which LC and EG values are considered.

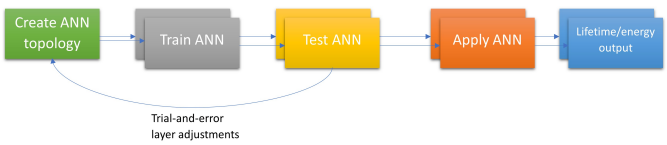

Fig. 9. Chronological application of networks. Feedback from network testing allowed for trial and error changes to layer structure.

are the same inputs to the electrothermal model. Once the networks have been trained, they can be applied to long term mission profile data directly, skipping the electrothermal modelling step.

Now that the tools for the prediction of long term lifetime consumption and energy generation have been described, Section IV proposes an algorithm for reducing lifetime consumption.

IV. Novel Active Thermal Control Algorithm

Active thermal control algorithms have become a more important area of research as the industry aims to maximise energy capture and device limits [10]. This paper proposes a novel ATC algorithm that works alongside an unchanged P&O MPPT algorithm.

Under normal conditions with no large fluctuations in average junction temperature, the standard P&O MPPT algorithm applies. Once the average junction temperature rise exceeds a defined threshold, the boost converter duty cycle is reduced according to the junction temperature rise, using Equation 5. The algorithm flowchart is seen in Figure 10.

$$D(i) = D(i-1) - \Delta D \cdot K \cdot \frac{\Delta T_j(i)}{L} \tag{5}$$

This equation is designed to decrease the current duty cycle by a value proportional to the ratio that the temperature rise ΔT_j exceeded the set limit L. L represents the temperature rise limit, in °C/s. A constant term K allows for more control over the magnitude of duty cycle adjustments. The influence of K is shown in Figure 11. ΔD is the magnitude change of the duty cycle per time-step in the standard P&O MPPT algorithm and is used as a scaling factor. With $K \cdot L / \Delta T_j = 1$, the ATC algorithm reduces the duty cycle by the same amount as an unchanged P&O algorithm.

Figure 12 shows the reduction in temperature rise when a step irradiance is applied. The temperature rise rate seen is larger than the set limit. This is due to the increase in irradiance, which causes a rise in power generation irrespective of the current operating point. If the change in irradiance is sufficient, all operating points will cause a temperature rise above the set limit L. As a result, the algorithm cannot slow this temperature rise. This can be partially improved with a stronger algorithm, with smaller values of L and larger values of K, however the algorithm can become unstable with values too extreme.

Figure 11 shows the algorithm results with consideration of different K values. The rate limit L is the dominant parameter for the rate of junction temperature increase, where the effect of K is not as pronounced.

Figure 12 demonstrates the effectiveness of the proposed algorithm, whereby the rate of junction temperature increase is decreased from $13.4°C/s$ using an unchanged MPPT algorithm to $4.1°C/s$. As expected, decreasing the rate limit L and increasing the constant parameter K correspond to making more common and dramatic changes to the duty cycle, shown by the decreasing rate of junction temperature increase. The different parameters show that tuning is capable

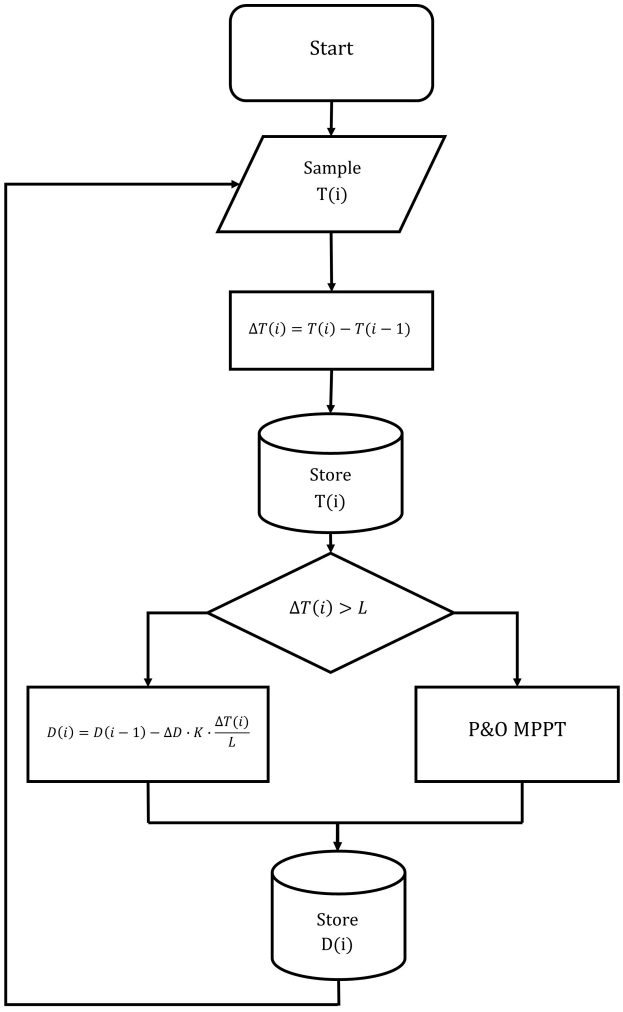

Fig. 10. Flowchart for proposed active thermal control algorithm. P&O MPPT algorithms have been widely implemented and documented within literature, and no suggestion is made for a specific implementation.

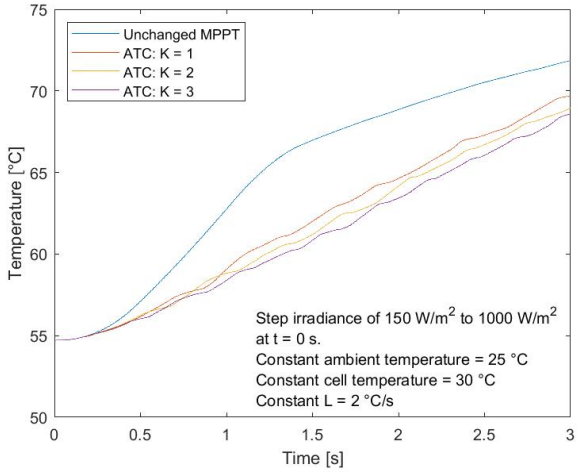

Fig. 11. Reduction in average junction temperature gradient when using proposed algorithm with differing K parameter under constant L, with step irradiance change of to 150 W/m^2 to 1000 W/m^2 .

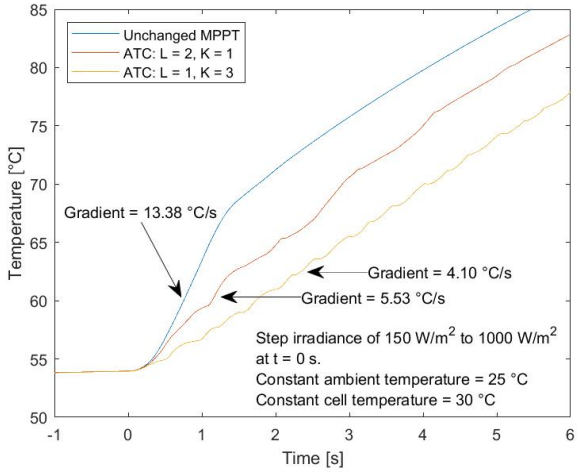

Fig. 12. Reduction in average junction temperature gradient when using proposed algorithm with different L and K parameters, under step irradiance change of to 150 W/m^2 to 1000 W/m^2 .

of adjusting the rate, which is related to the trade-off between MPPT speed (and therefore energy generation) and transistor damage accumulated. The slight variation in the temperature is a consequence of having the limit term L, such that the algorithm is cycling between on and off as the temperature rise fluctuates around the limit value. A lower limit is seen to cause a larger amount of variations, as it is more frequently switching between active and inactive states.

The average rate of junction temperature increase is higher than the set limit L for both cases in Figure 12. With a dramatic increase in irradiance such as the one used from 150 W/m^2 to 1000 W/m^2, the power flow will correspondingly increase dramatically. This means that, in effect, the temperature rise due to this increased power flow cannot be compensated or slowed sufficiently by the algorithm. As a result, the temperature rise rate will exceed the set limit. With smaller or slower increases in irradiance, the algorithm is capable of achieving the set rate limit.

V. Simulation and Network Training

The PV array is connected with 2 parallel strings with 9 series-connected panels on each string, with an array total open circuit voltage, V_{oc}, of 342.90 V and short circuit current, I_{sc}, of 37.12 A assuming identical panels.

The electrothermal model was implemented into Simulink using the Specialised Power Systems library.

The data used in this study is from the Baseline Measurement System dataset from the National Renewable Energy Laboratory's Solar Radiation Research Laboratory (SRRL) in Golden, CO, USA [29]. The irradiance data instrument is a CMP22 pyranometer inclined at 40-South measuring total solar irradiance. Ambient temperature is taken from the instrument deck. Cell temperature uses data from IKS-M 40-South, part of the SRRL PV Resource study. While this is not the same instrument as irradiance, it is believed that using this cell temperature would be a more accurate representation of the cell temperature when using the PV electrical model in this study than the case temperature for the CMP22.

TABLE I
System Electrical Design Parameters and Components

Quantity	Value
Rated power	10 kW
RMS grid voltage	240 V
Grid frequency	60 Hz
DC link voltage	450 V
DC link capacitor	2100 uF
PV capacitor	2100 uF
Inverter switching frequency	7.5 kHz
Boost converter	
Switching frequency	7.5 kHz
Inductor value	1.5 mH
LCL filter	
Inverter side inductor	8 mH
Capacitor	5 uF
Grid side inductor	4 mH
Datasheet components	
IGBTs	Infineon IKW40N60H3
PV panels	Trina Solar Vertex DE19 555W

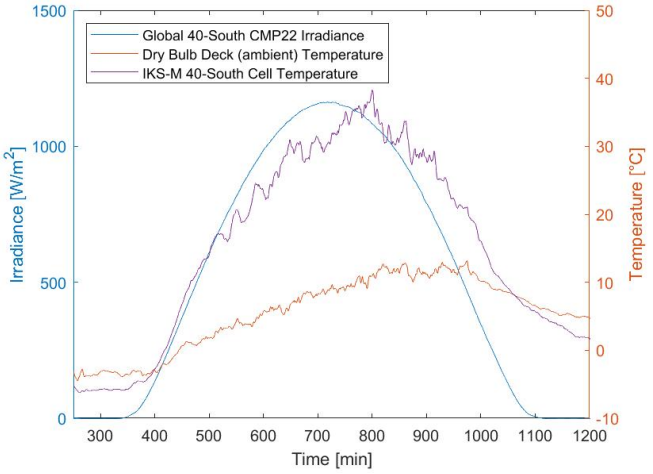

Fig. 13. An example of mission profile data used in the paper, taken from NREL data from March 31st 2021 [29]

365 days of data is used, starting 1st January 2021. Irradiance data below 1 W/m^2 was removed as this does not contribute significantly to energy generation and provides very minimal lifetime consumption while greatly increasing the amount of time required for simulations.

Training data was selected to best represent a range of conditions at this location, for irradiance and temperature. Testing data was selected at random. In total, 6 training days were used, totalling 3726 data points. 7 testing days were used, totalling 4762 data points.

Figure 14 shows examples from the 4 subsets of day: Clear, Overcast, Variable, and Very variable. These were sorted manually by considering peak irradiance and changes in irradiance. By applying the trained neural networks to each subset, it can be seen how the proposed algorithm functions under different conditions.

3 hidden layers were used, with each bracketed value in Table III denoting layer size. Layer structure can be seen in Figures 6 and 7. It was found that hidden layer structure was not critical to accuracy, provided the layers were sufficiently large. For example, the accuracy of a network with a structure

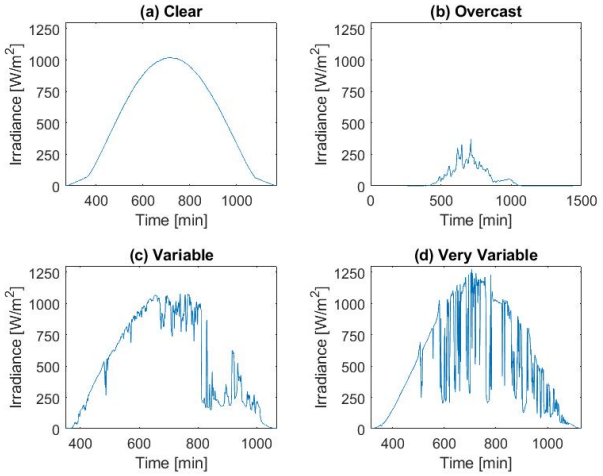

Fig. 14. Plots showing an example irradiance curve over a day sorted into groups: (a) Clear, (b) Overcast, (c) Variable, and (d) Very variable.

TABLE II
NUMBER OF DAYS IN EACH SUBSET

Day subset	Number of days
Clear	108
Overcast	30
Variable	136
Very variable	91

TABLE III
NEURAL NETWORK PARAMETERS

Network predictor	Hidden layer structure
LC	[10, 30, 1]
EG	[5, 20, 4]

of [10, 30, 1] had very little difference from that of [5, 40, 1]. Hidden layer activation functions were tanh for both LC and EG networks. Larger hidden layer sizes increase training computation time. No regularisation was used. Network inputs were standardised. Network target values were scaled to a range of 0 to 1.

Due to the statistical nature of network training, it was repeated 5 times in total. Each trained network was then applied to the testing data. The best performing network on the testing data was selected and applied to long-term data. Network performance was measured with the error percentage of total LC or EG to the simulated values. The equation can be seen in Equation 6. Networks chosen using Mean Squared Error (MSE), the performance metric used in fitrnet, proved to be less accurate, particularly in LC values. Using error percentages also gives a better understanding of accuracy, whereas MSE requires further context or comparison to understand.

$$\text{Error } \% = 100 \cdot |1 - \frac{\sum \text{Predicted LC or EG}}{\sum \text{Simulated LC or EG}}| \qquad (6)$$

Two sets of ATC parameters were tested, to show the trade-off between energy generation and lifetime improvement. The context for the relevant parameters is found in Section IV. The algorithms using the parameters from Table IV will be referred to as ATC no. 1 and 2. The ΔD value was a constant of 3×10^{-7} for the P&O and ATC algorithm. The reduction in junction temperature gradient for both of these sets of parameters can be seen in Figure 12.

TABLE IV
ATC PARAMETERS USED

ATC no.	L	K
1	2	1
2	1	3

VI. RESULTS AND DISCUSSION

In both simulation time and total data storage space requirements, the neural network method proposed in this paper is an overwhelming improvement on traditional electrothermal models for long term analysis. Where long term analysis is required, using neural networks would significantly speed up development processes, meaning more effective and time efficient design for reliability studies can take place. The speed improvements seen in Figure 15 and Table V when using the neural networks can be further improved by optimising the amount of training and testing data. The time required for either long term simulation or neural network training is dominated by the electrothermal model simulations, taking 99.8 % and 98.3 % of the total time respectively. However, reducing the amount of training data too far will result in low accuracy.

TABLE V
ESTIMATED TIME AND DATA STORAGE REQUIREMENTS TO SIMULATE 365 DAYS WORTH OF DATA USING SOLELY AN ELECTROTHERMAL MODEL NORMALISED TO PROPOSED NEURAL NETWORK REGRESSION METHOD.

Simulation type	Total time	Storage requirements
Electrothermal model	27.6	28.0
Proposed Neural Network	1	1

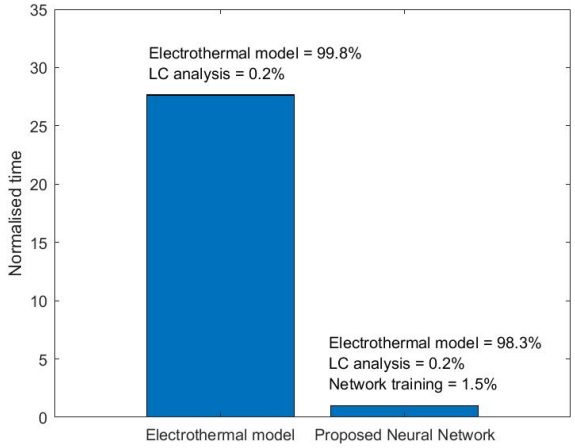

Fig. 15. Estimated time taken to simulate 365 days worth of data using solely an electrothermal model normalised to proposed neural network regression method, also showing breakdown into categories. Time taken to apply the neural network to the data is negligible.

It is only economical to use neural networks as outlined when the amount of data required to predict exceeds the amount of expected training and testing data. Otherwise, standard electrothermal models are sufficient. Using the example of this study, with 13 days of combined training and testing simulation, the benefits of using a neural network begins when 14 days or more are required.

Long term data of any length could be used with no further electrothermal simulations required. However lifetime consumption values would become less accurate with larger timescales as degradation would become more prominent, and no feedback metric for degradation is applied in this paper. One year of data is used here for a balance of maintaining accurate electrothermal properties, while also ensuring a mixture of conditions and long term performance is still analysed.

Due to the small sample size of electrothermal modelled days, and with training data being cherry-picked, the results in Table VI may not be representative of the long term trends. Additionally, small trends may be present in the electrothermal results, but in such limited quantity to appear insignificant in results. As a result, long term simulations show a better approximation of how it would operate if placed in the field.

TABLE VI
LC & EG PERCENTAGE CHANGE USING PROPOSED ATC ALGORITHM FROM TRAINING & TESTING ELECTROTHERMAL MODEL DATA RELATIVE TO AN UNCHANGED P&O ALGORITHM

MPPT algorithm	LC % change	EG % change
ATC no. 1	-1.34	-0.33
ATC no. 2	-5.42	-1.61

TABLE VII
NEURAL NETWORK REGRESSION ACCURACY IN PREDICTED VALUES AGAINST TESTING DATA

MPPT algorithm	Total testing error (%)		Correlation (%)	
	LC	EG	LC	EG
Unchanged	2.57	0.15	99.2	99.6
ATC no. 1	3.39	0.51	98.8	99.5
ATC no. 2	3.07	0.52	98.8	99.5

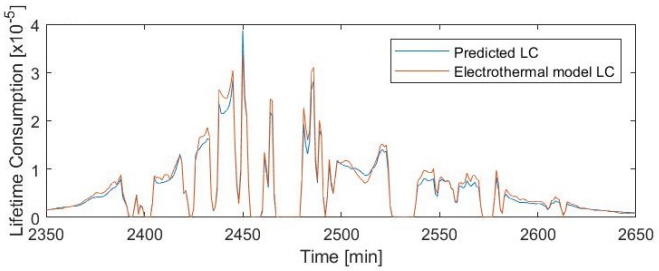

Fig. 16. An example comparison of predicted and electrothermal model lifetime consumption using testing data.

Figure 17 shows the accuracy of network predictions on the testing data. Ideally, the predictions and simulated results would be equal, therefore producing a linear line. As a result, deviation from the line demonstrates errors in the predictions. The plots clearly show the neural networks remain reasonably accurate for high lifetime consumption value predictions even

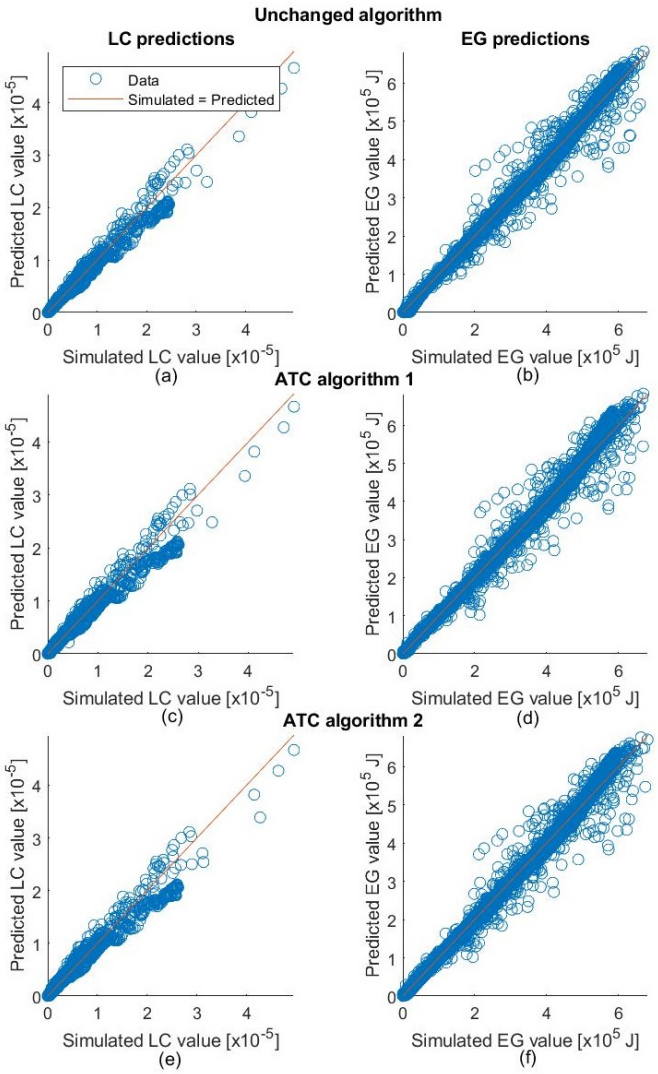

Fig. 17. Neural network predictions against simulated target values for both LC and EG, for the unchanged algorithm (a,b), proposed ATC algorithm no. 1 (c,d), and proposed ATC algorithm no. 2 (e,f). The accuracy and correlation values can be found in table VII.

with relatively few observations. There is an increasing amount of error in LC with increasing value, possibly due to the decreasing availability of training data for higher values. 72 % of simulated LC values were below 0.1×10^{-5}. EG can be seen as relatively easier to predict, with lower deviations from the ideal case. Energy generation, majoritively a function of irradiance, naturally sweeps through almost all values between 0 W/m^2 and its peak twice per day, whereas lifetime consumption, a more complex function, does not present such an easy target for training. This means that selecting accurate training data in the aim of optimising lifetime consumption training is non-trivial, and is the limiting step in overall network accuracy. This is demonstrated numerically in Table VII where the percentage LC error is up to 6 times higher than for EG.

In this study, the proposed neural network has been used to predict LC and EG values, with the later intention of comparing the outputs to determine the effectiveness of the proposed ATC algorithm. However the neural network demonstrated in this paper can be easily applied to any PV system.

While network training still requires an electrothermal model, it has demonstrated effectiveness in predicting values for long term data. Neural network predictions modelling PV systems could be used in the design and analysis stage of novel PV system designs or integration. Neural networks have already been applied to energy forecasting, however this paper also demonstrates the use for reliability studies [30]–[32].

TABLE VIII
LC & EG PERCENTAGE CHANGE WHEN USING PROPOSED ATC ALGORITHM WHEN APPLIED TO A YEAR LONG DATA SET RELATIVE TO AN UNCHANGED P&O ALGORITHM

MPPT algorithm	LC % change	EG % change
ATC no. 1	-1.08	-0.47
ATC no. 2	-3.26	-0.98

These results agree with electrothermal simulations with a demonstrated trade-off between lifetime improvement and energy generation, as shown by ATC no. 1 and 2. The parameters for the algorithm described in Section IV can be tuned for any compromise level between lifetime improvement and energy generation. There is a small decrease in LC change compared to Table VI. This could be explained by the cherry-picked data and small sample size as noted previously. However, these could also be explained by network inaccuracy.

While reducing the energy generation seems counter intuitive, it is offset by increasing the lifetime of the panel. The aim is to minimise the total cost of the system over its entire life, therefore the trade-off between lifetime improvement and energy generation demonstrated by the proposed algorithm can be used to find the optimal point. As mentioned, PV is set to play a large role in the decarbonisation of energy generation globally, and reducing the levelised cost of energy is key to this role.

The results of [18] showed a significant decrease in device lifetime models when a model for degradation feedback was included. Therefore, it is suspected that if these feedback models were applied to the ATC algorithm shown in this paper, the lifetime improvements over an unchanged algorithm would increase above those shown in this section.

TABLE IX
LC & EG PERCENTAGE CHANGE WHEN USING PROPOSED ATC ALGORITHM SPLIT BY DAY TYPE RELATIVE TO AN UNCHANGED P&O ALGORITHM

MPPT algorithm	LC % change	EG % change
Clear		
ATC no. 1	-1.14	-0.23
ATC no. 2	-1.59	-0.55
Overcast		
ATC no. 1	327.84	-7.13
ATC no. 2	-73.503	-5.77
Variable		
ATC no. 1	-2.08	-0.30
ATC no. 2	-4.26	-0.90
Very variable		
ATC no. 1	-1.09	-0.46
ATC no. 2	-4.43	-1.35

The high variation in LC seen for overcast days is due to lower absolute LC values. This causes network inaccuracies to become more prevalent on a percentage basis. Very variable days result in 39.2 times more lifetime consumed on average than overcast days, therefore in absolute value, improvements to overcast days are not critical. Clear days, on average, have 4.9 times greater peak solar hours compared to overcast days, where peak solar hours are equivalent to hours at an irradiance of 1000 W/m^2. This means, on average, there is approximately 4.9 times more energy generation over a clear day than overcast. Additionally, overcast days occur at a rate 3.6 times less frequently than clear days. Consequently, sub-par energy performance on overcast days does not significantly reduce total energy generation over a year.

TABLE X
COMPARISON OF LC & EG PERCENTAGE CHANGE WHEN USING PROPOSED ATC ALGORITHM WHEN APPLIED TO A YEAR LONG DATA SET RELATIVE TO AN UNCHANGED P&O ALGORITHM

Paper	LC %	EG %	Analysis duration
This paper	-3.3	-1.0	365 days
Andresen *et al.* [6]	-13	-3.7	10 minutes

Table X shows the advantage of this paper over existing literature. The LC and EG percentage changes for this paper are approximately a factor of 4 less, suggesting similar results to Andresen *et al.* could be achieved with careful consideration of the algorithm parameters. With a much longer analysis duration, more confidence can be given to the results, and a better understanding of the benefits over real world implementation can be ascertained. As mentioned previously, there are dramatic differences in the conditions over a year. Consequently, to suggest that results seen in Andresen *et al.* could hold throughout a year of mixed conditions would be incorrect. Using real irradiance data means that results in this paper, while may appear less impressive on face value, represent a more reality-true picture of the algorithm benefits.

An alternative form of the proposed algorithm could be used that increases the duty cycle rather than decreases it, taking advantage of the steeper negative gradient of power above the values for V_{MPP}. This is shown in Figure 18. This has the potential of more rapidly reducing the power output (and therefore junction temperature) while deviating less from the Maximum Power Point (MPP).

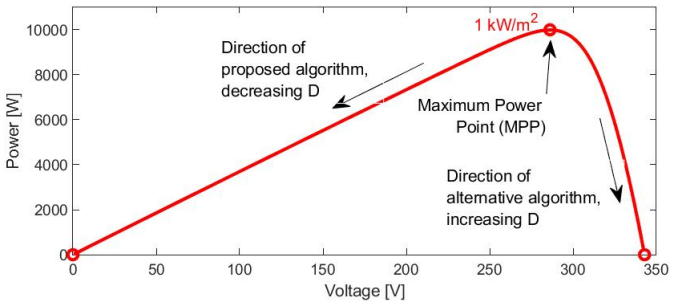

Fig. 18. Power-voltage plot for whole array, showing direction of operating point movement using proposed and alternative algorithms.

VII. CONCLUSIONS

This paper details the theory, implementation and results for a novel active thermal control MPPT algorithm utilising neural

networks for long term analysis. Current literature uses short analysis durations and non-real irradiance data, limiting the analysis of the effectiveness under real world conditions. In contrast, this paper implements long term analysis techniques and uses real meteorological data.

The proposed algorithm functioned as desired, reducing lifetime consumption values. A trade-off between lifetime improvements and energy generation was demonstrated. The algorithm parameters can be tuned to the designer's specifications. However it may have disadvantages in real-world implementation, as it requires accurate junction temperature measurement or estimation.

Neural networks were utilised to great effect for predicting lifetime consumption and energy generation values. Lifetime consumption was more difficult to accurately predict than energy generation. The results proved that this prediction method can be used for accurately modelling any PV system. Due to the requirement of electrothermal modelling for generating training and testing data, the time and storage benefits of using neural networks are only present when long-term predictions are needed.

Further work could include using a higher resolution data set, such as data sampled every second. One such data set is available from the National Renewable Energy Laboratory. This could potentially increase neural network accuracy, as it would increase the amount of training data by a factor of 60. Additionally, it would better represent real-world conditions, which could change on a second by second basis.

Monte Carlo analysis could be applied to the methods of this paper to find the expected B_{10} lifetime of the device. At present, only lifetime consumption is considered which does not take into account failure probability or statistical deviation.

REFERENCES

[1] V. Masson-Delmotte, P. Zhai *et al.*, "Summary for policymakers. in: Climate change 2021: The physical science basis. contribution of working group i to the sixth assessment report of the intergovernmental panel on climate change," Intergovernmental Panel on Climate Change (IPCC), Geneva, Switzerland, Tech. Rep., Oct. 2021.

[2] ——, "Summary for policymakers. in: Global warming of 1.5°c. an ipcc special report on the impacts of global warming of 1.5°c above pre-industrial levels and related global greenhouse gas emission pathways, in the context of strengthening the global response to the threat of climate change, sustainable development, and efforts to eradicate poverty," IPCC, Geneva, Switzerland, Tech. Rep., 2018.

[3] BEIS, "Net zero strategy: Build back greener," Department for Business, Energy & Industrial Strategy, London, UK, Tech. Rep., Oct. 2021.

[4] "Solar photovoltaics deployment," Department for Business, Energy & Industrial Strategy, 3 2022. [Online]. Available: https://www.gov.uk/government/statistics/solar-photovoltaics-deployment

[5] M. Thompson, C. Stark, C. C. Committee *et al.*, "Net zero - technical report," Committee on Climate Change, London, UK, Tech. Rep., May 2019.

[6] M. Andresen, G. Buticchi, and M. Liserre, "Thermal stress analysis and mppt optimization of photovoltaic systems," *IEEE Transactions on Industrial Electronics*, vol. 63, no. 8, pp. 4889–4898, 2016.

[7] J. Falck, C. Felgemacher, A. Rojko, M. Liserre, and P. Zacharias, "Reliability of power electronic systems: An industry perspective," *IEEE Industrial Electronics Magazine*, vol. 12, no. 2, pp. 24–35, 2018.

[8] H. Wang, D. Zhou, and F. Blaabjerg, "A reliability-oriented design method for power electronic converters," in *2013 Twenty-Eighth Annual IEEE Applied Power Electronics Conference and Exposition (APEC)*. IEEE, 2013, pp. 2921–2928.

[9] L. M. Moore and H. N. Post, "Five years of operating experience at a large, utility-scale photovoltaic generating plant," *Progress in Photovoltaics: Research and Applications*, vol. 16, no. 3, pp. 249–259, 2008.

[10] J. Kuprat, C. H. van der Broeck, M. Andresen, S. Kalker, M. Liserre, and R. W. De Doncker, "Research on active thermal control: Actual status and future trends," *IEEE Journal of Emerging and Selected Topics in Power Electronics*, vol. 9, no. 6, pp. 6494–6506, 2021.

[11] M. Andresen, K. Ma, G. Buticchi, J. Falck, F. Blaabjerg, and M. Liserre, "Junction temperature control for more reliable power electronics," *IEEE Transactions on Power Electronics*, vol. 33, no. 1, pp. 765–776, 2017.

[12] M. H. M. Sathik, J. Pou, S. Prasanth, V. Muthu, R. Simanjorang, and A. K. Gupta, "Comparison of igbt junction temperature measurement and estimation methods-a review," in *2017 Asian Conference on Energy, Power and Transportation Electrification (ACEPT)*. IEEE, 2017, pp. 1–8.

[13] N. Baker, M. Liserre, L. Dupont, and Y. Avenas, "Junction temperature measurements via thermo-sensitive electrical parameters and their application to condition monitoring and active thermal control of power converters," in *IECON 2013-39th Annual Conference of the IEEE Industrial Electronics Society*. IEEE, 2013, pp. 942–948.

[14] Z. Xu, F. Xu, and F. Wang, "Junction temperature measurement of igbts using short-circuit current as a temperature-sensitive electrical parameter for converter prototype evaluation," *IEEE Transactions on Industrial Electronics*, vol. 62, no. 6, pp. 3419–3429, 2014.

[15] E. R. Motto and J. F. Donlon, "Igbt module with user accessible on-chip current and temperature sensors," in *2012 Twenty-Seventh Annual IEEE Applied Power Electronics Conference and Exposition (APEC)*. IEEE, 2012, pp. 176–181.

[16] Y. Yang, A. Sangwongwanich, and F. Blaabjerg, "Design for reliability of power electronics for grid-connected photovoltaic systems," *CPSS transactions on power electronics and applications*, vol. 1, no. 1, pp. 92–103, 2016.

[17] C. Felgemacher, S. Araujo, C. Noeding, P. Zacharias, A. Ehrlich, and M. Schidleja, "Evaluation of cycling stress imposed on igbt modules in pv central inverters in sunbelt regions," in *CIPS 2016; 9th International Conference on Integrated Power Electronics Systems*. VDE, 2016, pp. 1–6.

[18] N.-C. Sintamarean, F. Blaabjerg, H. Wang, F. Iannuzzo, and P. de Place Rimmen, "Reliability oriented design tool for the new generation of grid connected pv-inverters," *IEEE Transactions on Power Electronics*, vol. 30, no. 5, pp. 2635–2644, 2014.

[19] P. D. Reigosa, H. Wang, Y. Yang, and F. Blaabjerg, "Prediction of bond wire fatigue of igbts in a pv inverter under a long-term operation," *IEEE Transactions on Power Electronics*, vol. 31, no. 10, pp. 7171–7182, 2015.

[20] S. Peyghami, T. Dragicevic, and F. Blaabjerg, "Intelligent long-term performance analysis in power electronics systems," *Scientific Reports*, vol. 11, no. 1, pp. 1–18, 2021.

[21] S. Wei, F. He, L. Yuan, Z. Zhao, T. Lu, and J. Ma, "Design and implementation of high efficient two-stage three-phase/level isolated pv converter," in *2015 18th International Conference on Electrical Machines and Systems (ICEMS)*. IEEE, 2015, pp. 1649–1654.

[22] IEEE Standards Association, "519-2014-ieee recommended practices and requirements for harmonic control in electric power systems," 2014.

[23] A. Bouzida, R. Abdelli, and M. Ouadah, "Calculation of igbt power losses and junction temperature in inverter drive," in *2016 8th International Conference on Modelling, Identification and Control (ICMIC)*. IEEE, 2016, pp. 768–773.

[24] "An5028: Calculation of turn-off power losses generated by an ultrafast diode," Application Note, ST Microelectronics, 2017.

[25] "An604: Calculation of conduction losses in a power rectifier," Application Note, ST Microelectronics, 2012.

[26] "An2015-10: Transient thermal measurements and thermal equivalent circuit models," Application Note, Infineon Technologies, 2020.

[27] R. Bayerer, T. Herrmann, T. Licht, J. Lutz, and M. Feller, "Model for power cycling lifetime of igbt modules-various factors influencing lifetime," in *5th international conference on integrated power electronics systems*. VDE, 2008, pp. 1–6.

[28] M. A. Miner, "Cumulative damage in fatigue," *Journal of Applied Mechanics*, 1945.

[29] A. Andreas and T. Stoffel, "Nrel solar radiation research laboratory (srrl): Baseline measurement system (bms)," National Renewable Energy Laboratory, Golden, CO, USA, Tech. Rep., 1981.

[30] F. Almonacid, C. Rus, P. Pérez, and L. Hontoria, "Estimation of the energy of a pv generator using artificial neural network," *Renewable Energy*, vol. 34, no. 12, pp. 2743–2750, 2009.

[31] F. Almonacid, P. Pérez-Higueras, E. F. Fernández, and L. Hontoria, "A methodology based on dynamic artificial neural network for short-term forecasting of the power output of a pv generator," *Energy Conversion and Management*, vol. 85, pp. 389–398, 2014.

[32] J. Ferrero Bermejo, J. F. Gomez Fernandez, F. Olivencia Polo, and A. Crespo Márquez, "A review of the use of artificial neural network models for energy and reliability prediction. a study of the solar pv, hydraulic and wind energy sources," *Applied Sciences*, vol. 9, no. 9, p. 1844, 2019.